Microsc. Microanal. 19, S5, 145–148, 2013
doi:10.1017/S143192761301252X

Microstructural Characterization of High Indium-Composition $In_XGa_{1-X}N$ Epilayers Grown on *c*-Plane Sapphire Substrates

Myoungho Jeong,[1] Hyo Sung Lee,[2] Seok Kyu Han,[2] Eun-Jung-Shin,[3] Soon-Ku Hong,[2,3,*] Jeong Yong Lee,[1] Yun Chang Park,[4] Jun-Mo Yang,[4] and Takafumi Yao[5]

[1]*Department of Materials Science and Engineering, Korea Advanced Institute of Science and Technology, Daejeon 305-701, Republic of Korea*
[2]*Department of Advanced Materials Engineering, Chungnam National University, Daejeon 305-764, Republic of Korea*
[3]*Graduate School of Green Energy Technology, Chungnam National University, Daejeon 305-764, Republic of Korea*
[4]*Measurement & Analysis Division, National NanoFab Center (NNFC), Daejeon 305-806, Republic of Korea*
[5]*Center for Interdisciplinary Research, Tohoku University, Sendai 980-8578, Japan*

Abstract: The growth of high-quality indium (In)-rich $In_XGa_{1-X}N$ alloys is technologically important for applications to attain highly efficient green light-emitting diodes and solar cells. However, phase separation and composition modulation in In-rich $In_XGa_{1-X}N$ alloys are inevitable phenomena that degrade the crystal quality of In-rich $In_XGa_{1-X}N$ layers. Composition modulations were observed in the In-rich $In_XGa_{1-X}N$ layers with various In compositions. The In composition modulation in the $In_XGa_{1-X}N$ alloys formed in samples with In compositions exceeding 47%. The misfit strain between the InGaN layer and the GaN buffer retarded the composition modulation, which resulted in the formation of modulated regions 100 nm above the $In_{0.67}Ga_{0.33}N$/GaN interface. The composition modulations were formed on the specific crystallographic planes of both the {0001} and $\{0\bar{1}14\}$ planes of InGaN.

Key words: nitride materials, InGaN, EDS, TEM, composition modulation

Introduction

III-nitride-based alloy materials have attracted attention for use in solar cell applications in addition to their optical device applications. $In_XGa_{1-X}N$ alloy materials are especially well used in GaN-based blue and white light-emitting diodes. However, few studies have focused on the solar cell applications of this alloy (Jani et al., 2007). To produce feasible solar cells with solar conversion efficiencies >50%, the materials used should have a band gap of about 2.4 eV. The band gap of InN was recently discovered to be 0.7 eV (Wu et al., 2002) as opposed to the previously believed 1.9 eV (Yodo et al., 2002). Considering the band gap energy of GaN is 3.4 eV, the band gap of a $In_XGa_{1-X}N$ material system covers nearly the entire solar spectrum (0.7–3.4 eV), thus enabling the design of multijunction solar cell structures with nearly the ideal band gap for maximum efficiency. However, many challenges still need to be overcome.

A major challenge is the epitaxic growth of high-quality single crystalline $In_XGa_{1-X}N$ alloys with entire indium (In) composition. In-rich $In_XGa_{1-X}N$ layers are not easily grown compared with gallium (Ga)-rich $In_XGa_{1-X}N$ layers because of the low dissociation temperature of InN. In addition, composition modulation or phase separation, such as multiphase InGaN (El-Masry et al., 1998), In metal clusters or droplets (Zhu et al., 2007), and InN formation (Doppalapudi et al., 1998), could occur because of the low miscibility between InN and GaN (Ho & Stringfellow, 1996). The large differences in the lattice parameters of GaN and InN, in the covalent radii of Ga and In, as well as in the formation enthalpy of GaN and InN, produce the large miscibility gap in the phase diagram of GaN and InN (Ho & Stringfellow, 1996). In this study, we characterized the microstructure of $In_XGa_{1-X}N$ layers with various In compositions under transmission electron microscopy, including the modulation of their In compositions.

*Corresponding author. E-mail: soonku@cnu.ac.kr

Materials and Methods

The $In_XGa_{1-X}N$ layers grown with various In compositions were prepared on (0001) *c*-plane sapphire substrates using plasma-assisted molecular beam epitaxy (PAMBE). After substrate cleaning (Lee et al., 2010), the substrates were introduced into a PAMBE system. Thermal cleaning of the substrates was carried out at 850°C for 60 min in the growth chamber, and then the substrates were exposed to nitrogen plasma with a radiofrequency (RF) power of 250 W at a flux rate of 0.8 sccm for 5 min, which converts the sapphire surface into an AlN nucleation layer (Moustakas & Molnar, 1993). Subsequently, a thin GaN buffer layer was grown at 770°C. During the growth of GaN buffer layer, the Ga beam equivalent pressure (BEP) was set to 1.1×10^{-7} torr, and a nitrogen plasma was maintained at a flux rate of 0.8 sccm with an RF power of 250 W. $In_XGa_{1-X}N$ layers about 500-nm thick were grown on the GaN buffer layer at 500°C, with the Ga flux corresponding to 1.1×10^{-7} torr BEP. In fluxes were changed to BEPs of 0.6, 1.6, 3.5, and 7.1×10^{-7} torr to grow $In_XGa_{1-X}N$ with various In contents.

High-resolution X-ray diffraction (HRXRD) was used to confirm the existence of the phase separation phenomenon using θ–2θ measurements. The microscopic structure was characterized under transmission electron microscopy (TEM; JEOL JEM 3010, operated at 300 kV) and aberration-corrected scanning transmission electron microscopy (STEM; JEM-ARM200F, operated at 200 kV) with a probe size of 0.5 nm. X-ray energy-dispersive spectroscopy (EDS) was utilized to observe composition changes.

Results and Discussion

The HRXRD in the θ–2θ scans (not shown) was used to determine the In composition of the $In_XGa_{1-X}N$ layers and to visualize the formation of the secondary phase, such as In metal, InN, multiphase InGaN, and an ordered structure. The In composition of InGaN was determined by the InGaN (0002) peak position using Vegard's Law. The determined In compositions of the $In_XGa_{1-X}N$ layers were 11% (at an In BEP of 0.6×10^{-7} torr), 33% (at a BEP of 1.6×10^{-7} torr), 47% (at a BEP of 3.5×10^{-7} torr), and 67% (at a BEP of 7.1×10^{-7} torr). All of the samples had no phase separated InN, In metal, and multiphase InGaN phase. However, the InGaN layers with In compositions of 47 and 67% showed additional satellite reflections around the InGaN (0002) peak (not shown). Such satellite reflections indicate that the InGaN layer has a superlattice-like inner structure (Moram & Vickers, 2009) caused by composition modulation, as shown in the TEM micrographs in Figures 1c and 1d.

Figure 1 shows a bright-field TEM micrograph of the $In_XGa_{1-X}N$ layers with In compositions (a) 11%, (b) 33%, (c) 47%, and (d) 67%. In Figure 1, the black arrow indicates the interface between the InGaN layer and the GaN buffer layer. Black and white fringes were observed in Figures 1c and 1d. These fringes formed through the composition modulation of In and Ga. The contrasts of the modulation are very clear for the sample with the higher In composition ($In_{0.67}Ga_{0.33}N$) compared with that of the $In_{0.47}Ga_{0.53}N$ sample. In addition, the thickness of the modulated layer is decreased as In composition increased. The reason for this is not clear at current status.

The generated lattice misfit between InGaN and GaN produces the strain within the InGaN layers, and contributes to the formation of the InGaN region without the composition modulations (Singh et al., 1997). As shown in the TEM micrograph (Fig. 1d), the modulations formed 100 nm above the InGaN/GaN interface and were not formed in the very initial growth region of InGaN, which implied that the misfit strain was large enough to prevent the composition modulation during the initial growth of InGaN. Also, a width from the InGaN/GaN interface to the modulation-starting point is roughly increased as increasing the In concentration as marked by the white vertical arrows in Figures 1c and 1d. It is caused by the increased misfit strain with the increased In composition, which retards the modulating phenomena.

Figure 2 shows a high-angle annular dark-field (HAADF) STEM micrograph and EDS line scan spectra from the composition-modulated region of the $In_{0.67}Ga_{0.33}N$ sample (Fig. 1d). From the EDS line scan spectra shown in Figure 2b, a simultaneous increase in In and decrease in Ga was observed across the black and white regions. The black and white contrasts in Figures 1 and 2 were clearly caused by composition modulation. The darker regions in the bright-field TEM micrograph (Fig. 1d) and the brighter regions in the HAADF-STEM micrograph (Fig. 2a) correspond to regions with high In content. The In concentration of the highly In segregated regions is about 80% compared with 60% for the remaining regions.

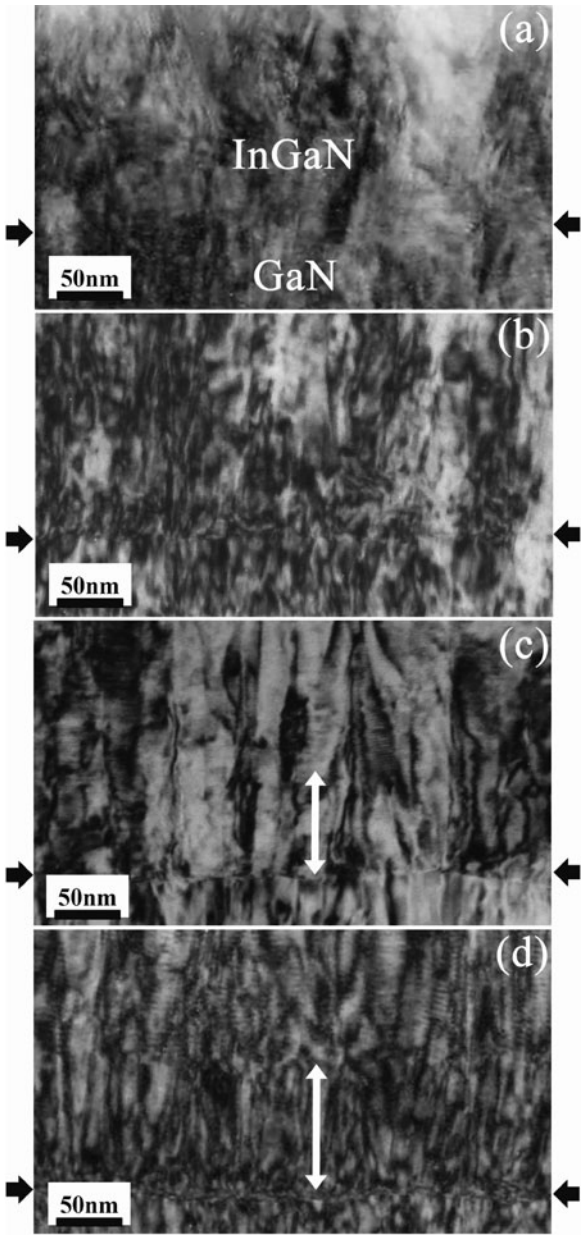

Figure 1. Bright-field transmission electron microscopy micrograph of the $In_XGa_{1-X}N$ layers with (**a**) 11%, (**b**) 33%, (**c**) 47%, and (**d**) 67% indium content. Horizontal black arrows indicate the positions of InGaN/GaN interface and white vertical arrows indicate the average height without modulation above the InGaN/GaN interface.

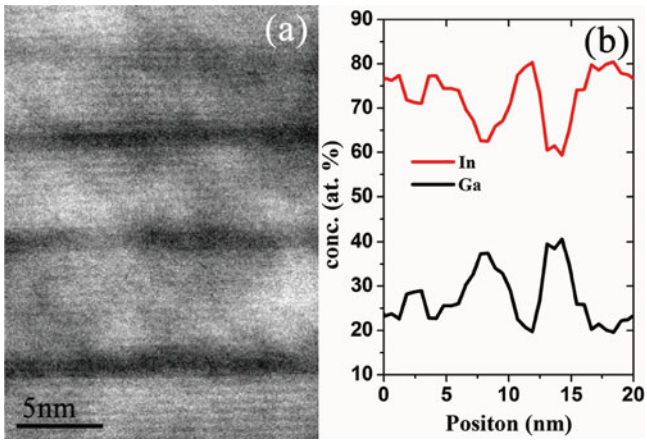

Figure 2. a: HAADF-STEM micrograph, and (**b**) EDS line spectra of the composition modulated region in the $In_{0.67}Ga_{0.33}N$ sample. HAADF, high-angle annular dark-field; STEM, scanning transmission electron microscopy; EDS, energy-dispersive spectroscopy.

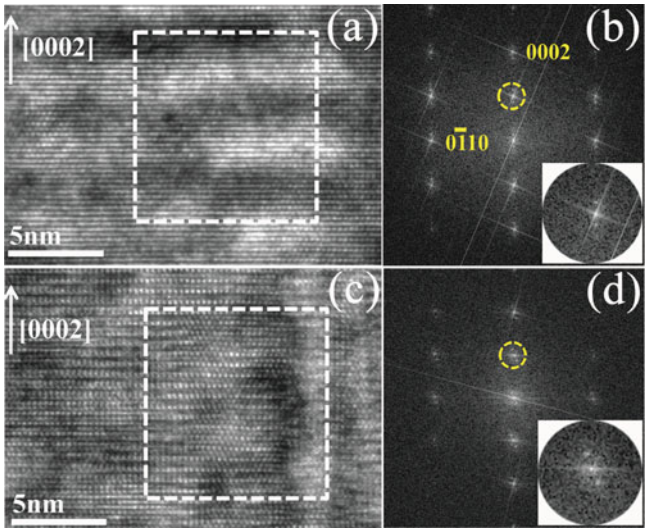

Figure 3. High-resolution transmission electron microscopy micrograph of the composition modulation within the $In_{0.67}Ga_{0.33}N$ layer. **a**: Typical distribution of composition modulation on *c*-planes, and the corresponding fast Fourier transform (FFT) image in (**b**). The inset image in (**b**) is the magnified 0001 (encircled) spot. **c:** Some areas have composition modulations on the $\{0\bar{1}14\}$ planes, and the corresponding FFT image is in (**d**). The inset image in (**d**) is the magnified 0001 (encircled) spot.

Figure 3 shows the high-resolution TEM (HRTEM) micrographs of the composition-modulated regions in the $In_{0.67}Ga_{0.33}N$ sample (Figs. 3a, 3c) and the digital diffraction patterns obtained using fast Fourier transform (FFT). The In atoms were segregated mainly on the *c* planes and on the planes inclined to the *c*-axis by about 65°. Figure 3a shows the composition modulations formed on the *c* planes, and the corresponding FFT image is shown in Figure 3b. In addition, Figure 3c shows the composition modulations formed on the planes inclined to the *c*-axis, and Figure 3d shows the corresponding FFT image. Each diffraction spot from the InGaN layer should be surrounded by extra diffraction spots for composition modulation because of the changes in lattice parameter and scattering coefficient. As shown in Figures 3b and 3d, satellite spots formed along the $\langle 0001 \rangle$ (Fig. 3b) and $\langle 0\bar{1}14 \rangle$ directions (Fig. 3d), which implies that the composition modulations formed mainly on the $\{0001\}$ and $\{0\bar{1}14\}$ planes. The $\{0001\}$ planes are dominant planes rather than $\{0\bar{1}14\}$ planes. However, other segregation planes except $\{0001\}$ and $\{0\bar{1}14\}$ planes were not observed. The modulated planes were not strict in the InGaN layer compared with other III–V compound semiconductors. For InGaP, InGaAsP (Henoc et al., 1982; Ueda et al., 1984), and InAlAs (Jun et al., 1996), the composition modulations formed along the $\langle 100 \rangle$ direction. The exact mechanism of composition modulation and the planes where the elements segregate are still unknown. As observed in Figure 1d, the InGaN layer shows that the columnar structure and alignment of the composition-modulated sublayers were changed across the column boundary. Given that the columnar-grown InGaN layer is affected by the morphology of the GaN buffer layer, the bumpy surface of the buffer layer may have affected the crystallographic planes on which the elements were segregated.

Conclusions

We studied the composition modulation phenomena in $In_XGa_{1-X}N$ layers grown by PAMBE with different In compositions. The $In_XGa_{1-X}N$ layers with In compositions >47% showed periodic composition modulations. Bright-field TEM and HAADF-STEM micrographs clearly revealed black and white contrasts caused by the different In compositions in the modulated regions. The EDS line scan spectra showed a simultaneous increase in In and decrease in Ga across the composition-modulated sublayers. The misfit strain between the InGaN layer and the GaN buffer layer retarded the composition modulation, which resulted in the appearance of the modulated regions 100 nm above the $In_{0.67}Ga_{0.33}N$/GaN interface. Detailed HRTEM studies revealed that the composition modulations were formed on the specific crystallographic planes of both $\{0001\}$ and $\{0\bar{1}14\}$ planes.

Acknowledgments

This work was supported by the National Research Foundation of Korea (NRF) grant funded by the Korea government (MEST; No. 2011-0016137).

References

Doppalapudi, D., Basu, S.N., Ludwig, K.F. & Moustakas, T.D. (1998). Phase separation and ordering in InGaN alloys grown by molecular beam epitaxy. *J Appl Phys* **84**, 1389–1395.

El-Masry, N.A., Piner, E.L., Liu, S.X. & Bedair, S.M. (1998). Phase separation in InGaN grown by metalorganic chemical vapor deposition. *Appl Phys Lett* **72**, 40–42.

Henoc, P., Izrael, A., Quillec, M. & Launois, H. (1982). Composition modulation in liquid phase epitaxial $In_xGa_{1-x}As_yP_{1-y}$ layers lattice matched to InP substrates. *Appl Phys Lett* **40**, 963–965.

Ho, I.-H. & Stringfellow, G.B. (1996). Solid phase immiscibility in GaInN. *Appl Phys Lett* **69**, 2701–2703.

Jani, O., Ferguson, I., Honsberg, C. & Kurtz, S. (2007). Design and characterization of GaN/InGaN solar cells. *Appl Phys Lett* **91**, 132117.

Jun, S.W., Seong, T.-Y., Lee, J.H. & Lee, B. (1996). Naturally formed $In_xAl_{1-x}As/In_yAl_{1-y}As$ vertical superlattices. *Appl Phys Lett* **68**, 3443–3445.

Lee, J.W., Kim, J.-H., Han, S.K., Hong, S.-K., Lee, J.Y., Hong, S.I. & Yao, T. (2010). Interface and defect structures in ZnO films on m-plane sapphire substrates. *J Crystal Growth* **312**, 238–244.

Moram, M.A. & Vickers, M.E. (2009). X-ray diffraction of III-nitrides. *Rep Prog Phys* **72**, 036502.

Moustakas, T.D. & Molnar, R.J. (1993). Growth of GaN by ECR-assisted MBE. *Physica B* **185**, 36–49.

Singh, R., Doppalapudi, D., Moustakas, T.D. & Romano, L.T. (1997). Phase separation in InGaN thick films and formation of InGaN/GaN double heterostructures in the entire alloy composition. *Appl Phys Lett* **70**, 1089–1091.

Ueda, O., Isozumi, S. & Komiya, S. (1984). Composition-modulated structures in InGaAsP and InGaP liquid phase epitaxial layers grown on (001) GaAs substrates. *Jpn J Appl Phys* **23**, L241–L243.

Wu, J., Walukiewicz, W., Yu, K.M., Ager III, J.W., Haller, E.E., Lu, H., Schaff, W.J., Saito, Y. & Nanishi, Y. (2002). Unusual properties of the fundamental band gap of InN. *Appl Phys Lett* **80**, 3967–3969.

Yodo, T., Yona, H., Ando, H., Nosei, D. & Harada, Y. (2002). Strong band edge luminescence from InN films grown on Si substrates by electron cyclotron resonance-assisted molecular beam epitaxy. *Appl Phys Lett* **80**, 968–970.

Zhu, X.L., Guo, L.W., Ge, B.H., Peng, M.Z., Yu, N.S., Yan, J.F., Zhang, J., Jia, H.Q., Chen, H. & Zhou, J.M. (2007). Observation of metallic indium clusters in thick InGaN layer grown by metal organic vapor deposition. *Appl Phys Lett* **91**, 172110.